KARMEN: NEUTRINO SPECTROSCOPY AT ISIS

G. DREXLIN
Institut f"ur Kernphysik I, Forschungszentrum Karlsruhe
D-76021 Karlsruhe, P.O. Box 3640, Germany
E-mail: guido@ik1.fzk.de

ABSTRACT

The Karlsruhe - Rutherford Neutrino Experiment KARMEN at the spallation neutron facility ISIS investigates fundamental properties of neutrinos as well as their interactions with matter. Low energy neutrinos with energies up to 50 MeV emitted by the pulsed ν - source ISIS are detected by a 56 tonne high resolution liquid scintillation calorimeter. Clear ν - signatures allow a reliable search for neutrino oscillations of the type $\nu_\mu \rightarrow \nu_e$ and $\bar{\nu}_\mu \rightarrow \bar{\nu}_e$ as well as a detailed investigation of neutrino - nucleus interactions in an energy range important for astrophysics. We present the results of the KARMEN experiment from data taking in the period from June 1990 - December 1995.

1 Introduction

Despite many attempts in the past sixty years to unravel the nature of the neutrino most of its intrinsic properties such as its rest mass and its possible inner structure resulting in a non-zero magnetic moment are still unknown. The study of fundamental neutrino properties has become a key issue in modern particle physics, nuclear physics and the new field of particle astrophysics. The most promising way to detect a non-zero neutrino mass is the search for *neutrino oscillations* which therefore has very actively been pursued in the past 15 years, however, no unambiguous positive evidence has been reported so far. In the field of particle astrophysics it is especially the investigation of *neutrino - nucleus interactions* which is important for the

understanding of various processes such as the ν-induced elemental synthesis in core-collapse supernovae explosions.

Whereas most neutrino experiments in the past have only been performed with high energy muon neutrinos in the multi-GeV range, precision experiments studying the above issues in neutrino physics can also be carried out with well-defined and copious sources of *low energy neutrinos* in the MeV range. The relevant neutrino energy region of up to 50 MeV is that of 'classical' nuclear physics. At these energies neutrino-nucleus cross sections are typically only of the order of 10^{-42} cm^2. Thus the extremely difficult experimental problem is to measure cross sections which are up to 20 orders of magnitude smaller than those from strong or electromagnetic background processes. In addition, the lack of suitable neutrino sources and the difficulties of high quality detection methods for low energy neutrinos have prevented neutrino physics to become a more systematic and sound working field.

But this situation has now improved due to two technical developments:
a) the completion of new high intensity *pulsed* proton accelerators (neutron spallation sources) providing intense bursts of different species of low energy neutrinos from the decays of pions and muons at rest
b) the possibility to build large volume liquid scintillation detectors with high resolution figures even down to a few MeV of energy deposit, supplemented by efficient background rejection systems.

The spallation neutron source ISIS at the Rutherford-Appleton Laboratory in England constitutes the first high intensity proton accelerator providing a pulsed neutrino source of that kind. Taking full advantage of the unique time structure of the ν-source ISIS, the large volume neutrino calorimeter KARMEN is investigating the fundamental properties of neutrinos via the search for neutrino oscillations in the two appearance modes $\nu_\mu \rightarrow \nu_e$ and $\bar{\nu}_\mu \rightarrow \bar{\nu}_e$. The study of neutrino-nucleus interactions, which is carried out simultaneously, is focused on the observation of charged and neutral current excitations of ^{12}C with special emphasis on the various implications for particle astrophysics. In the following we describe the basic features of the KARMEN neutrino experiment at ISIS [1] before presenting our results from five years of data taking.

2 The ISIS Neutrino Source

The spallation neutron facility ISIS at the Rutherford Appleton Laboratory is the most powerful pulsed neutrino source in operation. Two bunches of protons are extracted from the 800 MeV, 50 Hz proton synchrotron in a single machine cycle.

The DC-equivalent intensity is 200 μA. The beam is dumped in a Ta-D_2O target. Pions, produced in this target are stopped inside the target within 0.1 ns. Negative pions at rest are inevitably captured and absorbed by the target nuclei. Thus the consecutive decay sequences $\pi^+ \rightarrow \mu^+ + \nu_\mu$ and $\mu^+ \rightarrow e^+ + \nu_e + \bar{\nu}_\mu$ with both π^+ and μ^+ decaying at rest, are the ν-generating process of monoenergetic ν_μ (29.8 MeV) and of (ν_e, $\bar{\nu}_\mu$) with continuous energy distributions ranging up to 52.8 MeV ((fig. 1(a)). The neutrino flux is isotropic and of exactly the same intensity for all

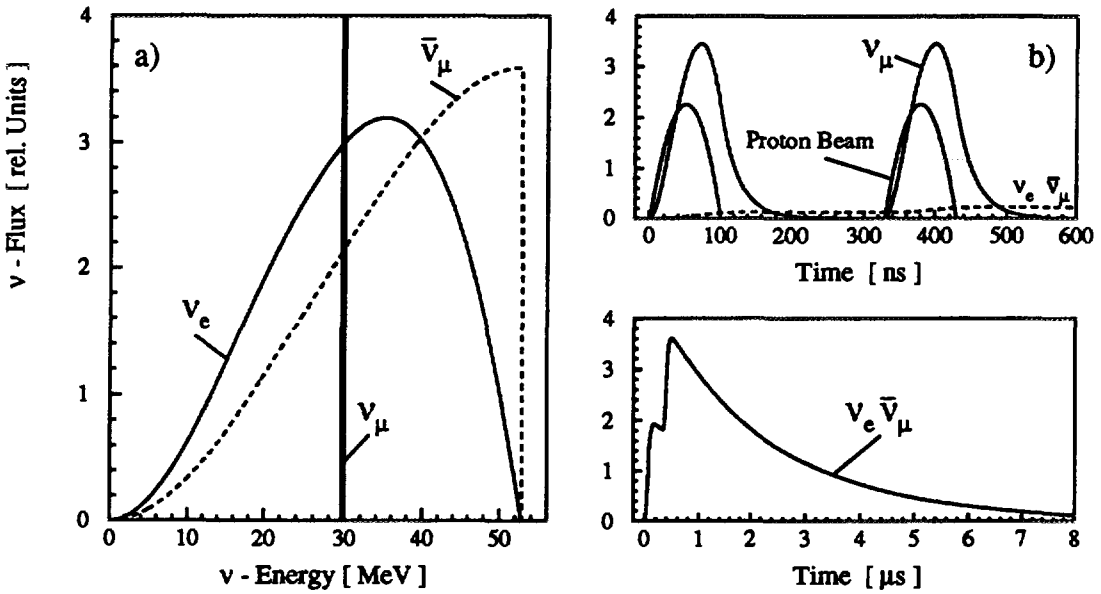

Figure 1: Energy spectra (a) and time structure (b) of the ISIS beam dump neutrino source.

three types of neutrinos. Contamination with $\bar{\nu}_e$ from the $\pi^- \rightarrow \mu^-$ decay chain is limited to 8×10^{-4}.

The beam's inherent time structure is uniquely matched with the different life time of π^+ (26 ns) and μ^+ (2.2 μs) (fig. 1(b)), resulting in high neutrino peak intensity and clear separation of ν_μ-induced reactions from those induced by ν_e or $\bar{\nu}_\mu$. The (ν_e, $\bar{\nu}_\mu$) inherit the decay time constant of the μ^+-decay, a significant identification label for reactions induced by these neutrinos. The accelerator duty cycle allows effective suppression of cosmic ray induced background by five orders of magnitude. This background can be analysed with highest precision during the 20 ms beam pause intervals.

3 The KARMEN Neutrino Spectrometer

The KARMEN detector is a 56 t segmented liquid scintillator calorimeter at a mean distance of 17.5 m (90°) from the beam stop [2]. A matrix structure of 32 rows × 16 columns subdivides the central detector into 512 independent modules. Each module is monitored by two 3-inch phototubes at each end side (fig. 2). Total internal light

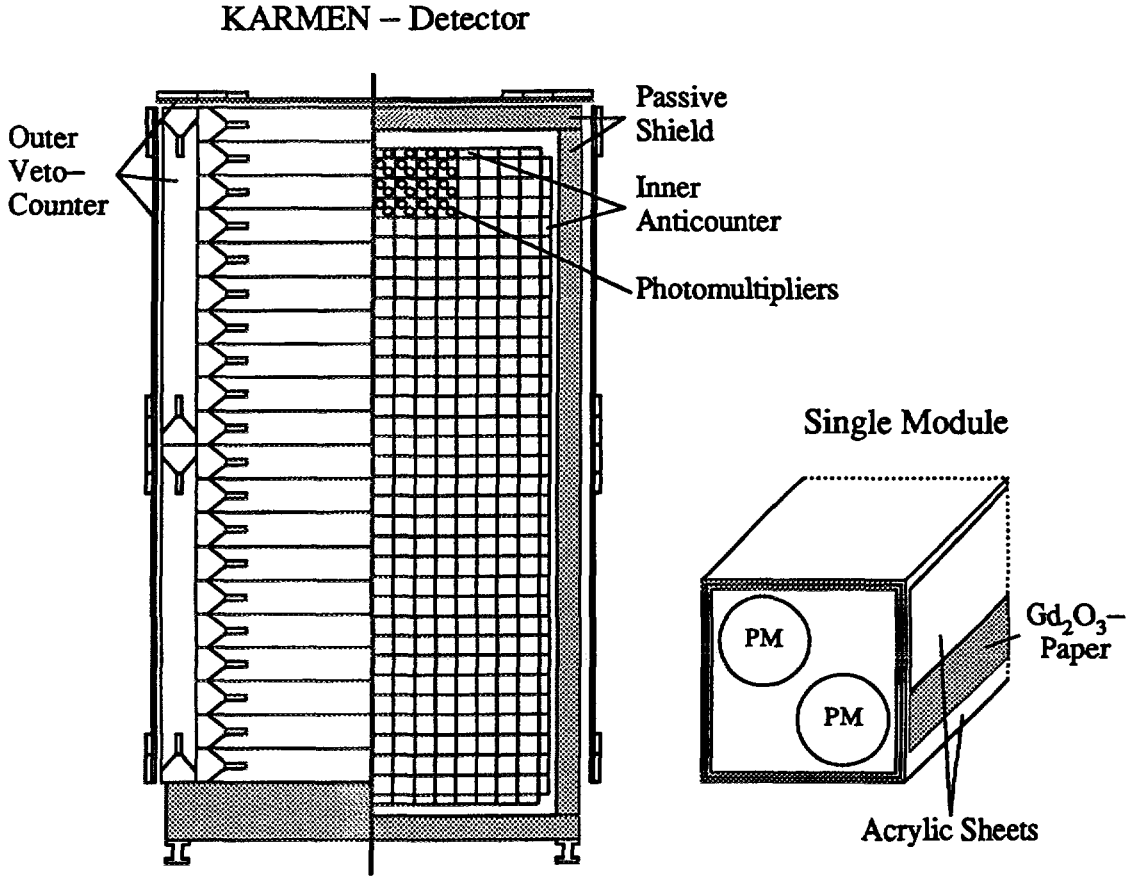

Figure 2: The 56 t high resolution liquid scintillator calorimeter KARMEN

reflection at the module walls is the mechanism of light transport within the modules (fig. 2inset). Gadolinium (Gd_2O_3), deposited in the module's walls, allows neutron detection through the Gd(n,γ) capture reaction releasing on average three gamma quanta with a sum energy of 7.6 MeV.

The liquid scintillator makes up more than 96% of the total mass of the central calorimeter. This essential design feature enables the calorimeter to account for

energy deposits of even less than 2 MeV. The average energy resolution is: $\sigma(E)/E = 11.5\%/\sqrt{E(MeV)}$.
The time resolution is 0.7 ns. A sandwich veto counter system rejecting cosmic muon induced background with 99.9% efficiency encloses the detector. A 7000 t steel blockhouse, lined inside with boracic polyethylene, provides effective shielding against neutrons from the spallation target and against the hadronic component of cosmic rays.

4 Neutrino Nucleus Interactions

The KARMEN liquid scintillation calorimeter consists entirely of hydrocarbons and thus serves as a massive live target of ^{12}C and ^{1}H nuclei for the investigation of various neutrino nuclear interactions. Inelastic scattering of neutrinos by nuclei can proceed either by the weak charged current (exchange of a $W^{\pm}$ boson) or by the weak neutral current (exchange of a Z^0 boson). In both cases the neutrino interaction gives rise to nuclear excitations which can be identified by the subsequent characteristic nuclear deexcitation processes [6].

At beam dump energies charged current reactions upon nuclei can only be induced by electron neutrinos due to energy conservation. An example is the socalled inverse β-decay reaction $\nu_e + {}^{12}C \rightarrow {}^{12}N_{g.s.} + e^-$. This transition, which is observed in the KARMEN experiment with negligible background, allows not only to identify electron neutrinos but also to measure for the first time their energy distribution.

On the other hand neutral current processes can be induced by all neutrino flavours on condition that their energy is above the reaction threshold. At ISIS all three neutrino flavours ($\nu_\mu, \nu_e, \bar{\nu}_\mu$) can induce the neutral current excitation $^{12}C(\nu,\nu')^{12}C^*$ (1^+1; 15.1 MeV) which therefore represents an ideal test case for the principle of flavour universality of the weak neutral current coupling.

In charged current (CC) as well as in neutral current (NC) neutrino scattering the nucleus can be used as a microscopic laboratory for the study of fundamental interactions and symmetries. The well defined change of quantum numbers in the nuclear transitions acts as an effective 'spin-isospin' filter and allows the study of the rather complex spin-isospin structure of the weak hadronic currents. In the charged current as well as in the neutral current excitation of ^{12}C the spin flip ($\Delta S = 1$) selects the axial-vector components of the weak hadronic currents, the change of isospin by one unit ($\Delta T = 1; \Delta T_3 = 0, 1$) correspondingly the isovector components. In this way only one spin-isospin component of the weak hadronic currents contributes in each reaction which thus can be measured with high accuracy.

The astrophysical implications of neutrino-nucleus interactions in the nuclear physics energy range is mainly connected with the new concept of ν-induced elemental synthesis in core-collapse supernovae. Nucleosynthesis in the overlying stellar burning shells of a supernova is induced by inelastic neutrino scattering exciting nuclei above their particle emission threshold. Neutrino scattering may be responsible for the production of most of the galactic abundances of ^{11}B, ^{19}F and various other elements, provided the neutrino interaction rates used in the model calculations are valid. Beam dump neutrinos emitted from the ISIS source are ideally suited to test these ideas, as they are the closest terrestrial analogon of core collapse neutrinos. An interesting example is the reaction $^{12}\mathrm{C}(\nu_e, e^-)^{12}\mathrm{N}^*$, which, on the one side is contributing to the ν-nucleosynthesis of ^{11}B , and which, on the other side can be measured reliably with the KARMEN experiment, making this reaction a test case for the relative contribution of the socalled 'ν-process' to elemental synthesis [5].

5 The Charged Current Reaction $^{12}\mathrm{C}(\nu_e, e^-)^{12}\mathrm{N}_{g.s.}$

The signature of the exclusive charged current reaction $^{12}\mathrm{C}(\nu_e, e^-)^{12}\mathrm{N}_{g.s.}$

$$\begin{array}{rcl} \nu_e + {}^{12}\mathrm{C} & \rightarrow & {}^{12}\mathrm{N}_{g.s.} + e^- \\ & & \downarrow \\ & & {}^{12}\mathrm{C}_{g.s.} + e^+ + \nu_e \end{array}$$

is a position-correlated, delayed coincidence of an electron from the inverse β-decay on ^{12}C within the ν_e time window of $0.5 - 10.5$ mus after beam-on-target and a positron from the subsequent β-decay of $^{12}\mathrm{N}_{g.s.}$ within the following 36 ms [4]. The Q-value of the initial reaction is $Q = -17.3$ MeV. The ^{12}N-decay, characterized by its lifetime of $\tau = 15.9$ ms and end point energy of $E_0 = 16.3$ MeV, uniquely identifies ν-induced transitions to the ground state of ^{12}N.

After software cuts on time, energy, position-correlation and background subtraction 498.4 ± 22.7 events remain. A fit to the time distribution relative to beam-on-targeet of the electrons with a time constant of $\tau_{exp.} = (2.21 \pm 0.18)\,\mu$s(fig. 3(c)), clearly indicates that these events are due to neutrinos from μ^+-decay. Background contamination (15.7 events) is almost negligible due to the unambiguous signature. The cross section for the charged current reaction averaged over the incident ν_e energy distribution ($0 - 52.8$ MeV) is:

$$< \sigma_{CC}(\nu_e) >_{exp.} \quad = \quad (9.3 \pm 0.4_{(stat.)} \pm 0.8_{(syst.)}) \times 10^{-42} cm^2$$

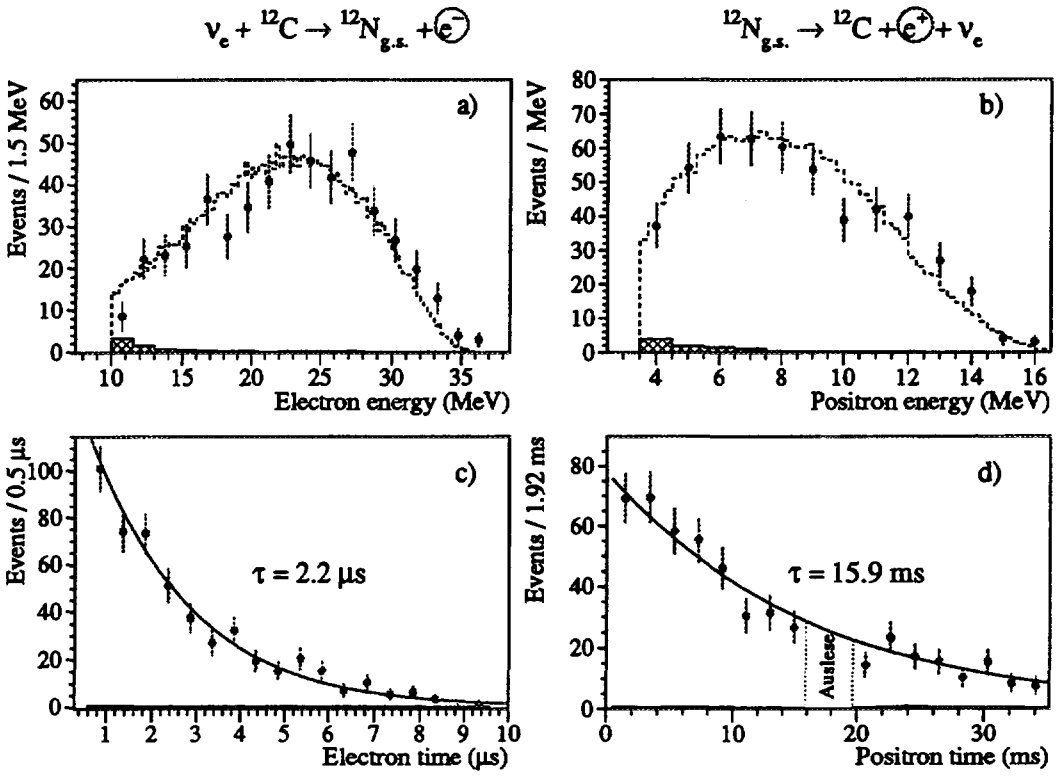

Figure 3: Energy and time distributions of the $^{12}C(\nu_e, e^-)^{12}N_{g.s.}$ reaction

in good agreement with theoretical predictions of $(8.0 - 9.4) \times 10^{-42}\,cm^2$.

The good calorimetric properties of the KARMEN detector also allowed for the first time a measurement of the energy dependence of the $^{12}C(\nu_e, e^-)^{12}N_{g.s.}$ cross section. As the recoil energy transferred to the ^{12}N nucleus is negligible, the neutrino energy E_ν is related to the electron kinetic energy E_{e^-} by $E_\nu = E_{e^-} + 17.3$ MeV. Thus a precise measurement of the electron kinetic energy determines the primary neutrino energy allowing the possibility of *neutrino spectroscopy*. The spectroscopic quality of the measured electron energy spectrum ensures a precise measurement of the spectral shape of ν_e emitted in μ^+-decay. Recently it has been shown that a precise determination of the ν_e shape parameter ω_L (the neutrino analogon to the famous Michel parameter ϱ) is sensitive to the Lorentz structure of muon decay. The experiment will therefore be able to set stringent upper limits on non V-A contributions in muon decay, especially to an interference amplitude of possible (non-standard model) scalar and tensor interactions in muon decay.

6 The Neutral Current Reaction $^{12}C(\nu,\nu')^{12}C^*(1^+,1)$

The neutral current reaction $^{12}C(\nu,\nu')^{12}C^*(1^+,1;15.1\,\mathrm{MeV})$, which has been observed for the first time in this experiment [3], can be induced by all three neutrino flavours present at ISIS. The signal for this excitation ^{12}C is the detection of 15.1 MeV gamma quanta from the decay of the excited $^{12}C^*(1^+,1)$ level. This level decays with a branching ratio of 96% via the emission of a single γ-ray back to the ground state, one therefore expects a clear peak structure around 15 MeV visible energy (fig. 4). The left part of figure 4 shows the energy distribution of neutrino

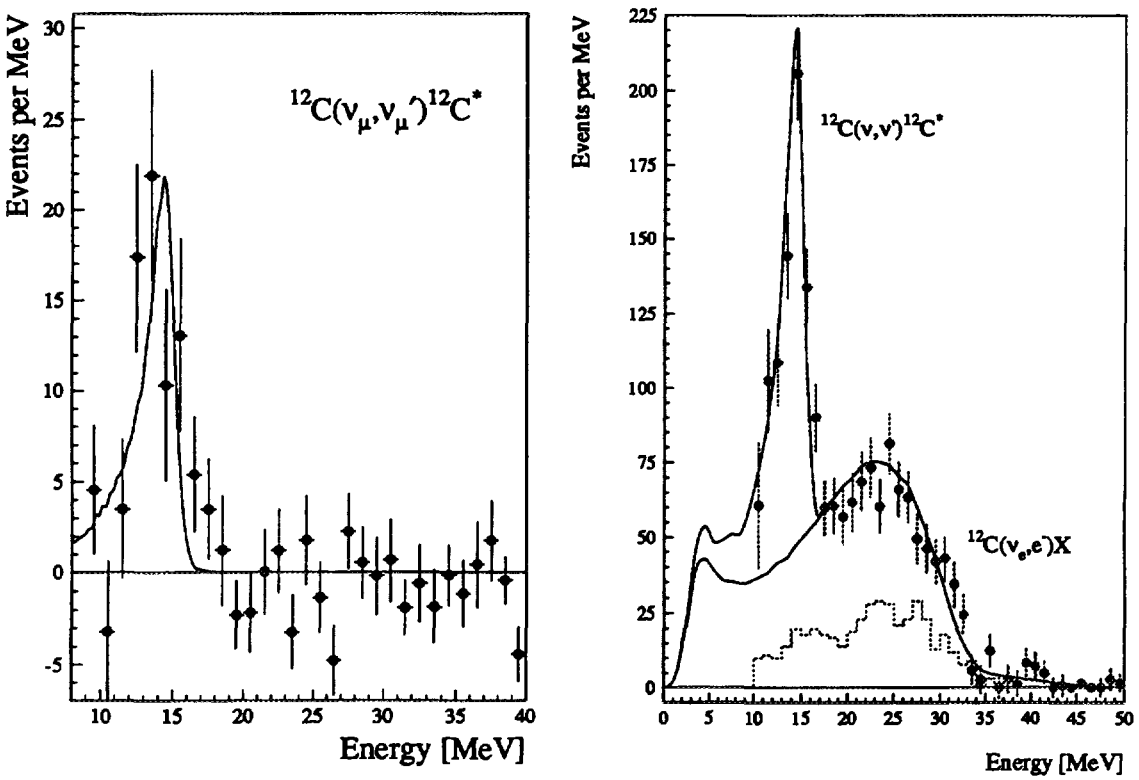

Figure 4: Visible energies of ν-induced single prong events, background subtracted.

induced events remaining after background subtraction in the narrow ν_μ-production time windows $0-100$ ns and $325-425$ ns after beam on target. Statistics for the ν_μ-induced excitation is still low due to the discrete ν_μ energy (29.8 MeV). Nevertheless the cross section for this reaction yields:

$$\sigma_{NC}(\nu_\mu)_{exp.} = (2.5 \pm 0.6_{(stat.)} \pm 0.4_{(syst.)}) \times 10^{-42} cm^2$$

with theoretical predictions of $(2.6-2.8) \times 10^{-42}\,\mathrm{cm}^2$ in good agreement.

The same data set as was used for the $^{12}C(\nu_e, e^-)^{12}N_{g.s.}$ reaction, has been scanned for neutral current events in the extended (ν_e, $\bar{\nu}_\mu$) time window from $0.6 - 90.6\,\mu s$. The energy distribution in the right part of figure 4 is the result of a likelihood analysis on the time distribution relative to beam-on-target of single prong events with an energy greater than 10 MeV, requiring a time signal of $2.2\,\mu s$ for excitations induced by the combined flux of ν_e and $\bar{\nu}_\mu$ and a time independent background. The energy spectrum clearly shows a peak due to the neutral current reaction $^{12}C(\nu, \nu')^{12}C^*(15.1\,MeV)$ in the range $11 - 16$ MeV. The broader underlying distribution has contributions from five reactions: neutrino-electron scattering and the inclusive charged current reactions $^{13}C(\nu_e, e^-)^{13}N$, $^{12}C(\nu_e, e^-)^{12}N_{g.s.}$, $^{12}C(\nu_e, e^-)^{12}N^*$ and $^{56}Fe(\nu_e, e^-)^{56}Co$. The cross section for the neutral current excitation of ^{12}C averaged over the energy spectra of ν_e and $\bar{\nu}_\mu$ is found to be

$$< \sigma_{NC}(\nu_e + \bar{\nu}_\mu) >_{exp.} = (10.9 \pm 0.8_{(stat.)} \pm 0.8_{(syst.)}) \times 10^{-42} cm^2$$

in good agreement with theoretical predictions of $(9.8 - 10.5) \times 10^{-42}\,cm^2$.

7 Search for $\nu_\mu \rightarrow \nu_e$ Oscillations

In the event of $\nu_\mu \rightarrow \nu_e$ oscillations, monoenergetic ν_e's would arise in the ν_μ time window after beam-on-target [7]. The detection reaction is $^{12}C(\nu_e, e^-)^{12}N_{g.s.}$ followed by the β–decay $^{12}N_{g.s.} \rightarrow {}^{12}C + e^+ + \nu_e$. One would therefore expect electrons with a peaked energy spectrum ($E_{e^-} = E_\nu - Q = 29.8 - 17.3 = 12.5$ MeV, see fig. 5a) within the two ν_μ time pulses (fig. 5b). The detection signature also contains the energy of the sequential spatially correlated e^+ (fig. 5c) which follows the e^- with the typical ^{12}N decay time (fig. 5d). The above measured number of CC reactions in the ν_e time window can be used to calculate the expectation of $\nu_\mu \rightarrow \nu_e$ induced CC reactions for $P_{\nu_\mu \rightarrow \nu_e} = 100\%$. Only the different detection efficiencies and the energy dependence of the cross section have to be taken into account to extract the ν-flux and cross section independent expectation of 187.8 oscillation signatures. Applying all cuts (e.g. $10 \leq E_{pr} \leq 14$ MeV; $0 \leq t_{pr} \leq 100$ ns or $325 \leq t_{pr} \leq 425$ ns) only 3 sequences are accepted within the data taken between July 1992 and December 1995. 0.45 ± 0.2 cosmic induced events contribute to the background which is dominated by the small contribution of ν_e's from μ^+–decay within the two 100 ns long ν_μ–time intervals after beam-on-target (1.76 ± 0.2). With a total background of $N_{bg} = 2.21 \pm 0.3$ events, there is no hint for $\nu_\mu \rightarrow \nu_e$ oscillations and an upper limit of the oscillation probability

$$P_{\nu_\mu \rightarrow \nu_e} < 4.8/187.8 = 2.6 \cdot 10^{-2} \qquad (90\%\,CL)$$

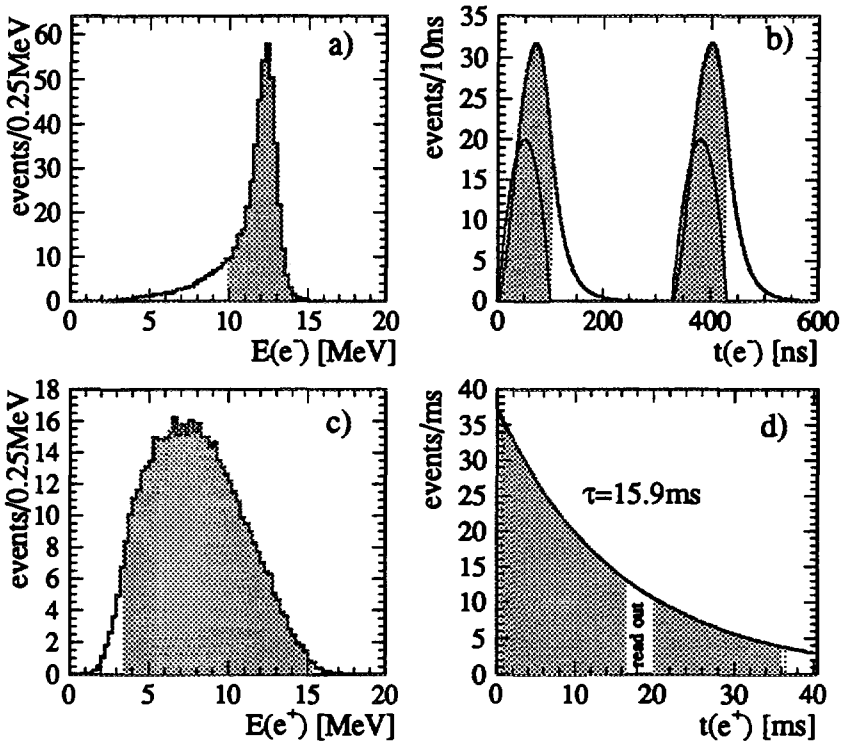

Figure 5: Expected signature for $\nu_\mu \rightarrow \nu_e$ full oscillation:
a) simulated MC energy of prompt event; b) proton pulses and time of prompt event relative to ISIS beam-on-target; c) MC energy of sequential event; d) time difference between prompt and sequential event; shaded areas show the allowed regions of evaluation cuts.

can be extracted following the PDG recommendations. Due to the normalization of the full oscillation expectation this result is very reliable. The background situation is very low so that the sensitivity for this oscillation channel is mainly limited by the relatively small expectation value for full oscillation, i.e. statistics.

8 Search for $\nu_e \rightarrow \nu_x$ Oscillations

The number of sequential events from the CC reaction $^{12}C(\nu_e, e^-)^{12}N_{g.s.}$ with subsequent ^{12}N-decay described in section 2.2 will be decreased in case of $\nu_e \rightarrow \nu_x$, $\nu_x = \nu_\mu, \nu_\tau$ whereas NC reactions $^{12}C(\nu, \nu')^{12}C^*(15.1\ \mathrm{MeV})$ which are also detected with KARMEN remain unchanged. Therefore the ratio of the extracted cross sections $R_{exp} = \frac{\langle\sigma\rangle_{NC(\nu_e+\bar{\nu}_\mu+\nu_\tau)}}{\langle\sigma\rangle_{CC(\nu_e)}} = 1.17 \pm 0.11$ should be increased with $\nu_e \rightarrow \nu_x$. A conservative comparison with theoretical predictions of $R_{theo} = 1.08 \pm 0.02$ doesn't show a statistical significant higher value so that an upper limit of the oscillation probability $P_{\nu_e \rightarrow \nu_x} < 0.197$ ($90\%\,CL$) can be deduced. This limit is nearly inde-

pendent on flux calculations or uncertainties of the theoretical cross section because only their ratios are used [8].

Due to the energy dependence of the oscillation probability not only a reduction of the event rate but also a distortion of the energy spectrum of the prompt e^- and its spatial distribution results from $\nu_e \rightarrow \nu_x$. With the good detector resolution in energy and space, a shape analysis provides even more stringent upper limits for $sin^2(2\Theta)$ in the energy-space sensitive range of $\Delta m^2 = 3 \ldots 30\,\mathrm{eV}^2$ (see fig. 9).

9 Search for $\bar{\nu}_\mu \rightarrow \bar{\nu}_e$ Oscillations

Apart from a small contamination ($\bar{\nu}_e/\nu_e < 6 \cdot 10^{-4}$), $\bar{\nu}_e$'s are not produced in the ISIS target. The detection of $\bar{\nu}_e$'s would therefore indicate oscillations $\bar{\nu}_\mu \rightarrow \bar{\nu}_e$ in the appearance channel. The signature for the detection of $\bar{\nu}_e$'s is a spatially correlated delayed coincidence of positrons from $\mathrm{p}(\bar{\nu}_e, \mathrm{e}^+)\mathrm{n}$ with energies up to $E_{e^+} = E_{\bar{\nu}_e} - Q = 52.8 - 1.8 = 51\,\mathrm{MeV}$ (fig. 6b) and γ emission of either of the two neutron capture processes $\mathrm{p}(\mathrm{n},\gamma)\mathrm{d}$ or $\mathrm{Gd}(\mathrm{n},\gamma)\mathrm{Gd}$ with γ energies of 2.2 MeV or up to 8 MeV, respectively (fig. 6d). The positrons are expected in a time window of 0.5 to 10.5 μs after beam-on-target (fig. 6a). The neutrons from $\mathrm{p}(\bar{\nu}_e, \mathrm{e}^+)\mathrm{n}$ are thermalized and captured typically within $\tau = 120\,\mu\mathrm{s}$ (fig. 6c). The neutron detection efficiency for the analyzed data is 23.8%. The data set remaining after applying all cuts in energy, time and spatial correlation is shown in fig. 7. A prebeam analysis of cosmic ray induced sequences results in an accumulated background level of 11.0 ± 0.2 events per μs in the prompt 10 μs–window (see fig. 7a). The actual rate is $14.7 \pm 1.2/\mu\mathrm{s}$ which corresponds to a beam excess of $2.3\,\sigma$ compared with the prebeam level including ν_e induced CC (8 events) and $\bar{\nu}_e$ contamination (1.1 events). Although the secondary part of the sequences shows the typical signature of thermal neutron capture, the prompt time and energy distribution does not follow the expectation from $\bar{\nu}_\mu \rightarrow \bar{\nu}_e$ oscillation with $\Delta m^2 = 100\,\mathrm{eV}^2$.

To extract a possible small contribution of $\bar{\nu}_\mu \rightarrow \bar{\nu}_e$, the data set is scanned with a two-dimensional maximum likelihood analysis on time and energy distribution of the positrons requiring a 2.2 μs exponential time constant for the e^+ and a time independent cosmic induced background. The measurement of the e^+ energy with spectroscopic quality is highly sensitive to changes in the energy spectrum due to the dependence of the oscillation probability on the mass term Δm^2 (see fig. 8a). The energy distributions of the positrons used in the likelihood analysis therefore have been tested with spectra for Δm^2 in the range from 0.01 to $100\,\mathrm{eV}^2$. The results of this maximum likelihood analysis are shown in fig. 8b.

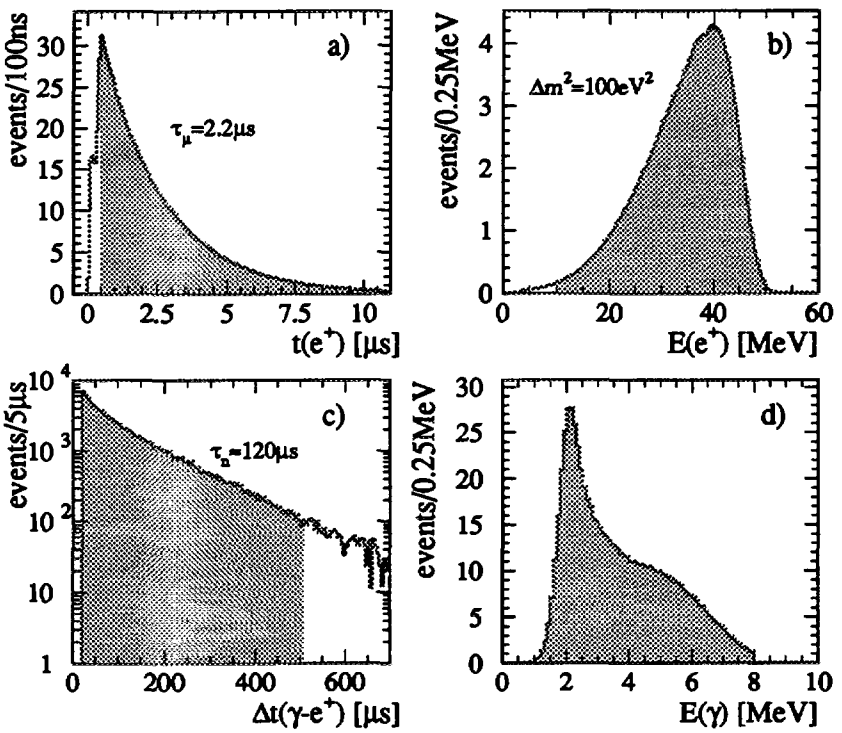

Figure 6: Expected signature for $\bar{\nu}_\mu \rightarrow \bar{\nu}_e$ full oscillation:
a) time of prompt event relative to ISIS beam-on-target; b) MC energy of prompt positron for $\Delta m^2 = 100\,\mathrm{eV}^2$; c) time difference between prompt e^+ and sequential γ's; d) energy of sequential γ's; shaded areas are accepted by evaluation cuts.

Over the entire parameter range of Δm^2 investigated there is no evidence for oscillations resulting in a $90\%\,CL$ upper limit for a possible oscillation signal of 10 to 14 events, depending on Δm^2. This confirms that the beam excess has no oscillation signature in time and energy of the prompt events. Our result can be compared with an expected signal of 6 to up to more than 40 events based on a recently published oscillation probability of $P_{\bar{\nu}_\mu \rightarrow \bar{\nu}_e} = 0.0034$ by LSND [9]. For large Δm^2 we expect at KARMEN 1547 detected oscillation events for full oscillation which results in an upper limit of the mixing angle

$$sin^2(2\Theta) < 11.6/1547 = 7.5 \cdot 10^{-3} \quad \text{for large } \Delta m^2 \qquad (90\%\,CL\,).$$

Fig. 9 shows the KARMEN exclusion curves in the parameter space of Δm^2 and $sin^2(2\Theta)$ in a two neutrino flavor oscillation calculation for the appearance channels $\nu_\mu \rightarrow \nu_e$ and $\bar{\nu}_\mu \rightarrow \bar{\nu}_e$ in comparison with some other results of ν–oscillation searches at accelerators and reactors.

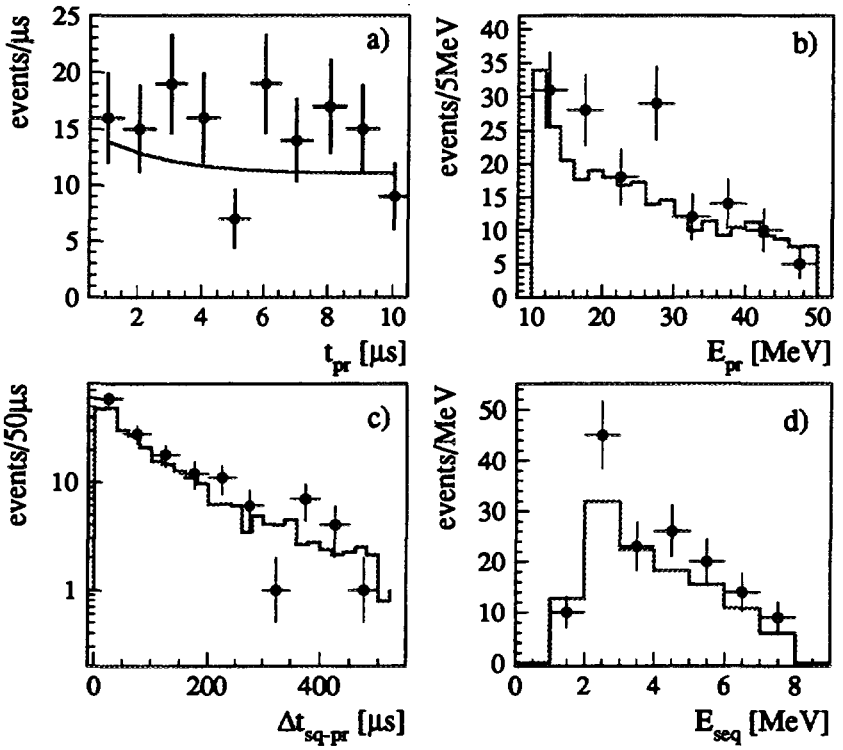

Figure 7: Time (a,c) and energy (b,d) distribution of reduced sequences; lines and histograms represent the pre-beam background (11.0 events per μs) plus ν_e-induced CC events and $\bar{\nu}_e$-contamination.

10 KARMEN Upgrade

Whereas the sensitivity for $\nu_\mu \rightarrow \nu_e$ oscillations is essentially limited by statistics, the KARMEN sensitivity in the $\bar{\nu}_\mu \rightarrow \bar{\nu}_e$ channel can be dramatically increased by the reduction of the small but dominant cosmogenic background (see fig. 7). Detailed investigations and MC simulations showed that this background is induced by cosmic muons being stopped or undergoing inelastic scattering in the iron blockhouse which surrounds the KARMEN detector and veto system. Energetic neutrons emitted in these processes can penetrate deeply into the detector without triggering the veto system, thus producing an event sequence of prompt recoil protons followed by the capture of the then thermalized neutrons. To mark the original muons in the vicinity of the detector, a further active veto layer within the blockhouse, 1 m away from the existing shield, is being built since the beginning of 1996 [10]. All sides of the detector will be covered by plastic scintillator bars with an overall surface of 300 m^2. This new veto system will reduce the cosmogenic sequential background by a factor of 40.

In addition to this veto system, an increase of the neutron detection efficiency

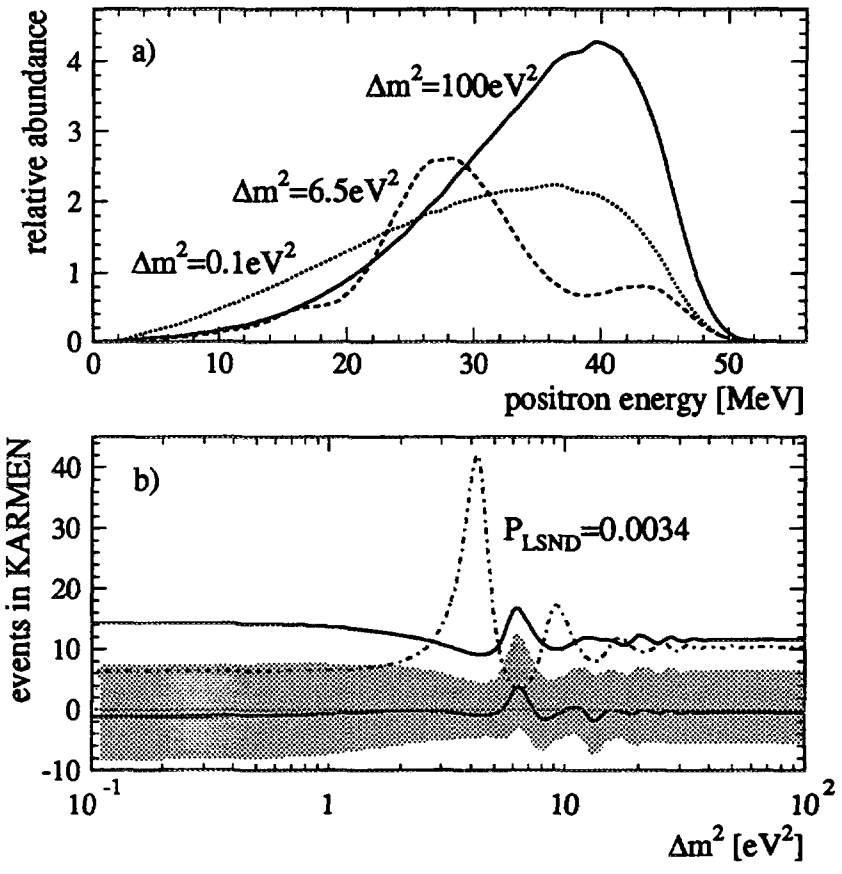

Figure 8: a) Examples of expected e^+–spectra (visible energy including detector response) for different oscillation parameters Δm^2; b) likelihood-fit results depending on Δm^2; the shaded area represents the 1σ–error band around the best fit values for $\Delta m^2 = 0.01 \ldots 100\,\mathrm{eV}^2$; the solid line above the shaded band shows the 90% CL upper limit from KARMEN, the broken line the expected event numbers in KARMEN based on the LSND oscillation evidence.

as well as improvements of the trigger system are envisaged. After two years of further measuring time, the KARMEN sensitivity for $\bar{\nu}_\mu \rightarrow \bar{\nu}_e$ is expected to cover the whole parameter region of evidence suggested by LSND. Fig. 9 also shows the expected exclusion curve from the upgraded KARMEN experiment if no oscillation signal will be found. The veto upgrade will also increase the signal to background ratio in the investigation of the recently published anomaly in the time distribution of ν–induced single prong events.

The KARMEN experiment has found no positive evidence for ν–oscillations in neither of the investigated channels $\nu_\mu \rightarrow \nu_e$ and $\bar{\nu}_\mu \rightarrow \bar{\nu}_e$ or $\nu_e \rightarrow \nu_x$. The upper limit for $\nu_\mu \rightarrow \nu_e$ is very reliable due to the spectroscopic measurement of the ν_e–flux from μ^+–decay at ISIS and the nearly background-free $^{12}\mathrm{C}\,(\,\nu_e\,,\mathrm{e}^-\,)\,^{12}\mathrm{N}_{g.s.}$ detection re-

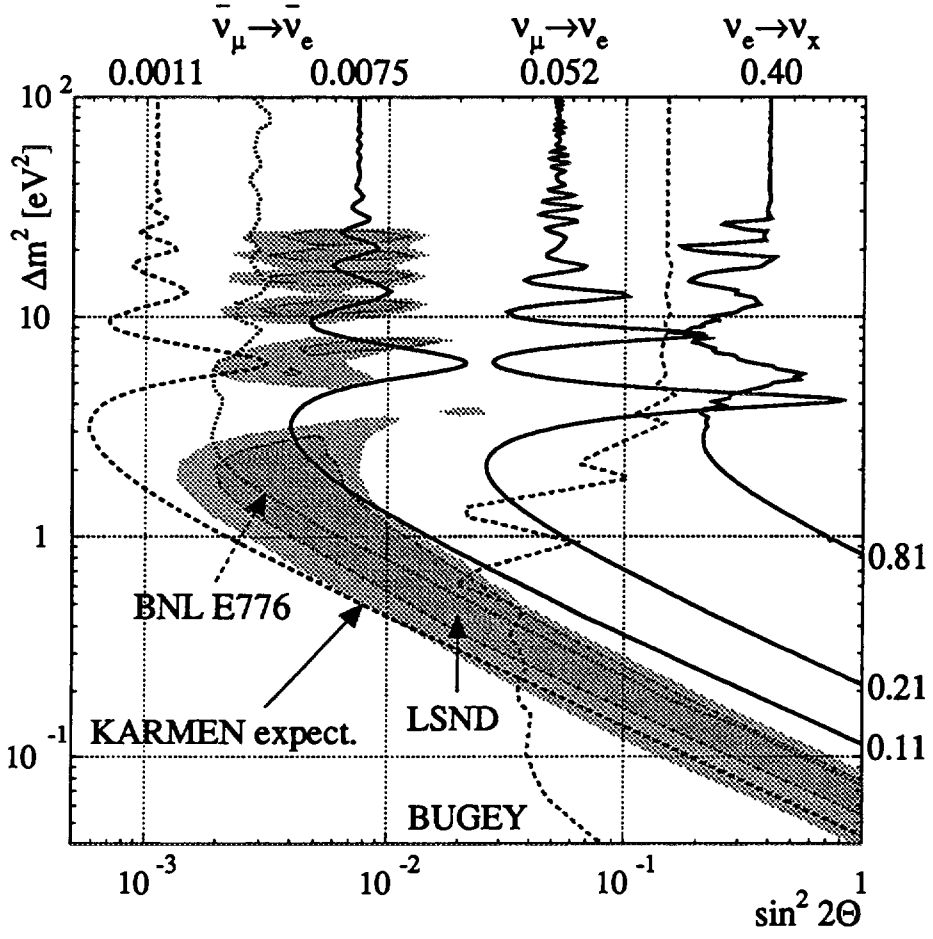

Figure 9: 90% CL exclusion curves and limits for $\Delta m^2 = 100\,\mathrm{eV}^2$, $sin^2(2\Theta) = 1$ from KARMEN for $\nu_\mu \to \nu_e$, $\bar{\nu}_\mu \to \bar{\nu}_e$ and $\nu_e \to \nu_x$ as well as the expected sensitivity for $\bar{\nu}_\mu \to \bar{\nu}_e$ after the upgrade; oscillation limits from BNL E776 and Bugey; LSND evidence is shown as shaded areas (90% CL and 99% CL areas respectively).

action. The sensitivity of the search for $\bar{\nu}_\mu \to \bar{\nu}_e$ is actually limited by cosmogenic background, but will be increased substantially by the current upgrade of the experiment. A sensitivity of $sin^2(2\Theta) \approx 1 \cdot 10^{-3}$ for large Δm^2 will be reached by the end of 1998.

Acknowledgement

This work was supported, in part, by the Bundesministerium für Bildung, Wissenschaft, Forschung und Technologie.

References

[1] B. Zeitnitz, *Prog. Part. and Nucl. Physics* **13** (1985) 445.

[2] G. Drexlin et al., *Nucl. Instr. Meth.* **A 289** 490-495 (1990).

[3] B. Bodmann et al., *Phys. Lett.* **B 267** 321-324 (1991).

[4] B. Bodmann et al., *Phys. Lett.* **B 280** 198-203 (1992).

[5] S. E. Woosley et al., *Astrophys. J.* **356** 272-301 (1990).

[6] B. Zeitnitz, *Prog. Part. Nucl. Phys.* **32** (1994) 351.

[7] G. Drexlin, *Prog. Part. Nucl. Phys.* **32** (1994) 375.

[8] K. Eitel et al., *Proc. of the XIIIth Rencontres de Blois*, June,8-12 1996, to be published

[9] C. Athanassopoulos et al., *Phys. Rev. Letters* **75** (1995) 2650.
C. Athanassopoulos et al., *Phys. Rev. Letters* **77**, (1996) 3082.

[10] G. Drexlin, B. Zeitnitz *Proposal for an Upgrade of the KARMEN Veto System*, Internal KARMEN Report